Skin perfusion photography

Citation: Satat, Guy, Christopher Barsi, and Ramesh Raskar. "Skin Perfusion Photography." 2014 IEEE International Conference on Computational Photography (ICCP) (May 2014), Santa Clara, Calif. p.1-8.

As Published: http://dx.doi.org/10.1109/ICCPHOT.2014.6831804

Publisher: Institute of Electrical and Electronics Engineers (IEEE)

Persistent URL: http://hdl.handle.net/1721.1/92732

Version: Author's final manuscript: final author's manuscript post peer review, without publisher's formatting or copy editing

Skin Perfusion Photography

Guy Satat Christopher Barsi Ramesh Raskar
MIT Media Lab
guysatat@mit.edu

Abstract

The separation of global and direct light components of a scene is highly useful for scene analysis, as each component offers different information about illumination-scene-detector interactions. Relying on ray optics, the technique is important in computational photography, but it is often underappreciated in the biomedical imaging community, where wave interference effects are utilized. Nevertheless, such coherent optical systems lend themselves naturally to global-direct separation methods because of the high spatial frequency nature of speckle interference patterns. Here, we extend global-direct separation to laser speckle contrast imaging (LSCI) system to reconstruct speed maps of blood flow in skin. We compare experimental results with a speckle formation model of moving objects and show that the reconstructed map of skin perfusion is improved over the conventional case.

1. Introduction

Generally, the radiance of a scene contains two components. Direct light is the component that is due to the illumination of an observation point by the source itself. Global light is the component due to illumination from other scene points and can be further classified into several categories, such as inter-reflections, subsurface scattering, translucency, and volumetric scattering. Global and direct light components contain valuable information about a scene, and their separation allows for the mitigation and exploitation of this information, for example, to characterize materials or to study light interaction with a scene.

Global and direct components are especially important in biological imaging. Direct reflections are used to infer surface properties, whereas global light is used to understand volumetric properties of the sample. Usually, because computational photography techniques are underappreciated in these fields, global-direct separation is effected using expensive hardware and complex experiments.

One particular example of multi-component light transport occurs in the case of laser speckle contrast imaging (LSCI), which is a wide-field technique for reconstructing speed maps of blood flow in biological media [9]. In this technique, coherent light illuminates a biological sample. The surface roughness, on the order of the optical wave-

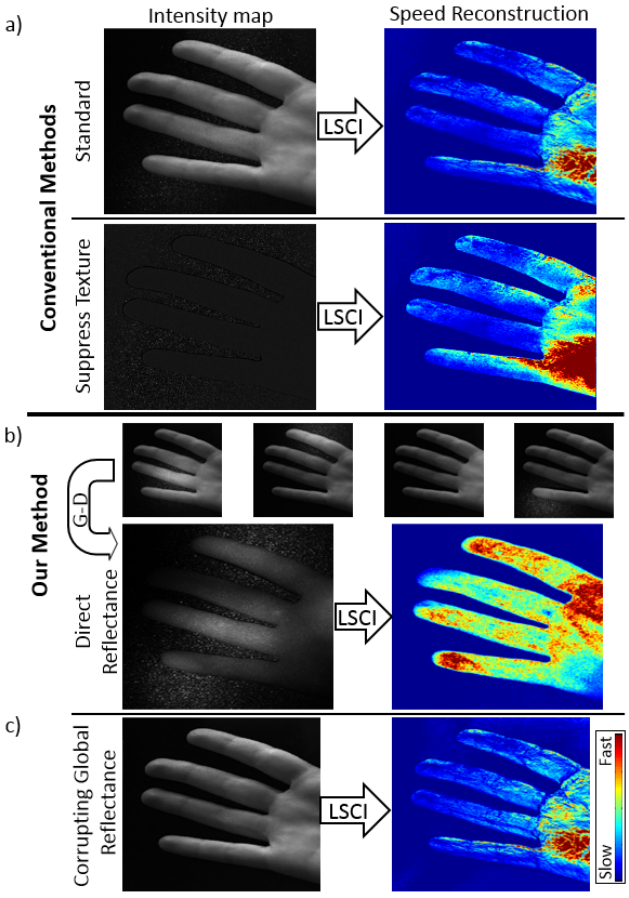

Figure 1. Global-direct separation improves measurement of skin perfusion. a) Standard methods compute skin perfusion from a speckle interference pattern. b) Using multiple images, we separate the global light (the subsurface) and reconstruct a more accurate, uniform skin perfusion map. c) The global component corrupts the conventional methods.

length, scatters the light in many directions. The result is a high-frequency interference pattern called speckle (Fig. 2, left). Although speckle is often an unwanted effect in imaging [19, 27], it can be used for measuring relative speeds of scattering objects. For a fixed object, the speckle pattern is time-invariant, and the resulting image has a very high contrast. For a dynamic object, the speckle pattern varies during the camera exposure time, washing out the final image. Thus, speckle contrast is directly related to the flow velocity of the scattering materials (Fig. 2, right).

An important application of LSCI is the measurement of skin perfusion, which determines blood flow in skin, and is used to monitor burns, wounds, and skin lesions. Unfortunately, however, scattering from the underlying tissue corrupts the contrast measurement. Here, we present the application of global-direct separation methods to coherent illumination to simplify and improve measurement of blood flow. The technique requires a hardware implementation that utilizes the natural high-frequency interference pattern of laser speckle to separate the desired component from the corrupting tissue scattering.

1.1. Contributions

Specifically, our contributions include

1. a generalization of global-direct separation to wave-based imaging,
2. an application of global-direct separation in skin perfusion measurement, and
3. a hardware implementation to demonstrate the principle.

Limitations: Currently, we model speckle scattering from a statistical perspective, rather than with a wave equation. This allows us to model random speckle phenomena without having to fully generalize global-direct separation to the wave optics regime, but its extension to deterministic systems remains an open question.

1.2. Related Work

LSCI theory was proposed by Fercher and Briers [9] after significant statistical analysis [11]. Several modifications and extensions to speckle modeling have been demonstrated [8, 10, 12, 34], but deriving rigorous quantitative results remains an open question [8].

LSCI implementation was first used to analyze microvasculars in the retina [9] and has been applied to cerebral tissues (usually on rats) [5, 17, 18, 20]. Advancements have included dual-wavelength systems for studying microvascular activity in burns [25] and multiple exposures to use speckle temporal statistics for improving spatial resolution [6] or contrast of cerebral flow through the skull [18].

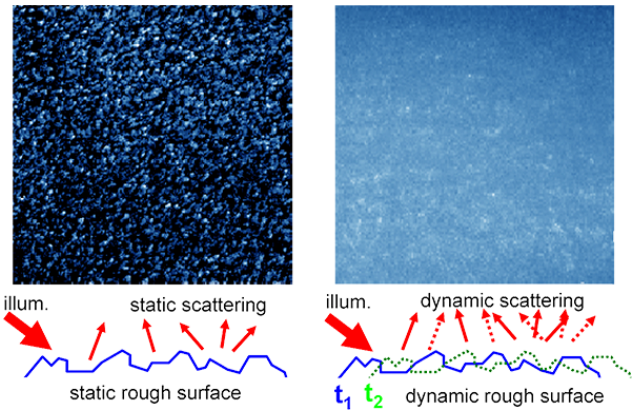

Figure 2. Left: speckle formation from a rough static surface has high contrast. Right: Speckle formation from a rough dynamic surface produces low contrast images.

Rege et al. suggest anisotropic numerical processing for increased SNR [26]. Our global-direct separation improves skin perfusion maps and can be integrated with these methods with, e.g., a high-speed camera or projector.

Skin perfusion analysis via LSCI was suggested by Briers [4]. A similar system was suggested later [29]. Analysis of wound healing in pigs was performed recently [30]. Commercial devices [24] exist for medical use. A recently conducted quantitative comparison of skin perfusion measurements between a full field laser Doppler imager (see below) and a commercial device concluded that a multi-exposure device offers some advantages [31].

Doppler-based methods are alternatives to LSCI. In this technique, time-resolved sensors are used to measure the Doppler shift of scattered light. Briers, however, showed that LSCI and Doppler methods are equivalent [3], except that LSCI has better sensitivity at low speeds, and that Doppler methods account for multiple scattering. A recent work [10] uses laser Doppler for flowmetry in skin and suggests a model for quantitative analysis. Doppler sensitivity has been improved in combination with ultrasound [33].

Global-direct separation can be effected through high-frequency illumination [21] and has been enhanced recently [13, 16]. O'Toole et al. [22] demonstrated a hardware-based global-direct solution using dual coding. Achar [1] addressed the issue of moving objects during global-direct separation by registering frames captured with high frequency illumination patterns. Global-direct separation was used for medical imaging for enhancing veins in skin imaging [15]. The present work performs global-direct separation of coherent light, which naturally produces a high-frequency illumination pattern via wave interference. The direct component is used for improved imaging of skin perfusion.

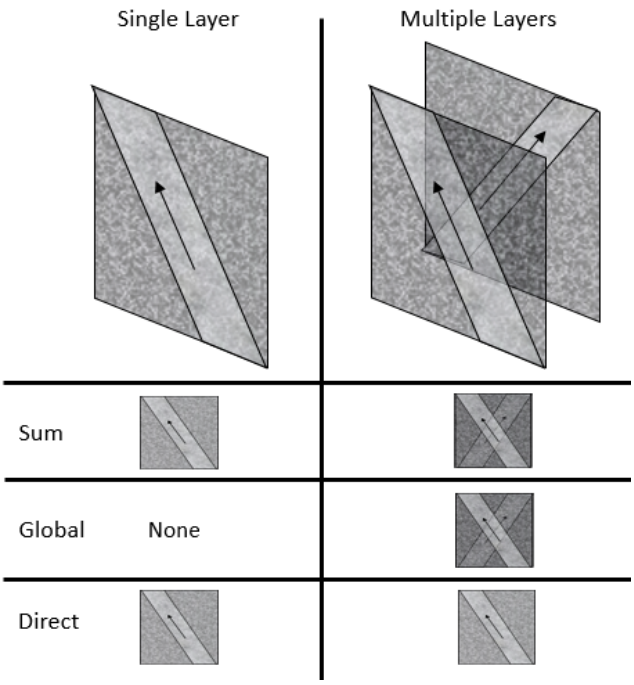

Figure 3. Global light produces erroneous contrast maps for skin perfusion. Left: a single layer of dynamic scattering can be reconstructed easily. Right: a second layer compounds the contrast image, and the resulting speed map is incorrect.

2. Theory and Method

2.1. Speed Estimation Using Speckle

Diffractive optics considers the wave properties of light. For coherent light propagation, relative phase delays result in an interference pattern. When coherent light scatters from a rough surface (feature size $\sim$ optical wavelength), many coherent light components add randomly at an observation point. This de-phased sum results in a granular, high frequency interference pattern called speckle (Fig. 2). The speckle contrast at a pixel (i, j) is

$$K_{ij} = \frac{\sigma_{ij}}{\mu_{ij}}, \tag{1}$$

where μ_{ij} is the mean and σ_{ij} is the per-pixel standard deviation of the intensity, both calculated over a spatial window around a given pixel. Typically, speckle intensities follow negative exponential statistics, so that, theoretically, $K = 1$. To calculate K for a given image, we calculate μ_{ij} and σ_{ij} for an $M \times M$ window around pixel (i, j). A typical experimental contrast map is shown in Fig. 1.

If the scattering object moves, the generated speckle pattern will vary dynamically. For short times, the speckle pattern changes little, but after a characteristic time τ_c, the speckle pattern becomes completely uncorrelated from the initial configuration. Photographing the speckle image with an exposure time T longer than τ_c will yield a blurred image (Fig. 2, right). The contrast becomes [2]

$$K(T) = \sqrt{\beta \left\{ \frac{\tau_c}{T} + \frac{\tau_c^2}{2T^2} \left[\exp\left(\frac{-2T}{\tau_c} \right) - 1 \right] \right\}}, \tag{2}$$

where β is a constant that depends on the ratio of pixel size to speckle size. Importantly, the underlying motion of the scattering objects determines τ_c and, consequently, the contrast. For example, a fast moving object with speed V will have a small τ_c, and the resulting photograph will have very low contrast (Fig. 2). Because of the underlying assumptions, the specific form of Eq. 2 is not universally accepted [23], so it is more common to assume [28] that $\tau_c \ll T$ and $V \sim \lambda/\tau_c$. This allows us to reconstruct the speed as a function of contrast and exposure time:

$$V \sim (K^2 T)^{-1} \tag{3}$$

In LSCI, we measure blood flow in skin (skin perfusion) by observing the speckle patterns produced by moving red blood cells. As blood flows, the cells undergo random Brownian motion to produce a time-varying speckle pattern. Measuring the contrast allows us to reconstruct the speed map of the flow. However, because light penetrates the skin, scattering occurs also from tissue and capillaries beneath the skin. This scattering corrupts the contrast measurement and results in an incorrect speed map.

Eq. 3 provides the inverse relationship between scatterers' speeds and image contrast for skin perfusion [28]. To summarize, the standard LSCI procedure is: (1) illuminate a sample with coherent light; (2) record a speckle pattern for exposure time T; (3) use Eq. 1 to calculate the speckle contrast; and (4) reconstruct the speed map via Eq. 3.

2.2. Global-Direct Separation for Coherent Illumination

We utilize global-direct decomposition to improve skin perfusion maps by removing light components scattered from beneath the skin. Consider the simplified schematic in Fig. 3: for a single skin layer, LSCI is straightforward. However, underlying tissue (modeled in Fig. 3 (right) as a second scattering layer) makes an unwanted speckle contribution to the contrast image.

In the context of skin perfusion, therefore, the global component is due to subsurface and volumetric scattering (Fig. 4). Accepted separation techniques [21] capture multiple images of the scene, which is illuminated with different high frequency patterns. Thus, a set of intensity values are associated with each pixel (i, j). The maximum value (L^+) and the minimum value (L^-) can be used to separate

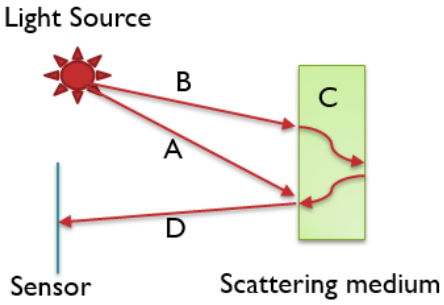

Figure 4. Light rays are captured from both the surface and subsurface. The sensor measures the intensity of D, which is a result of direct illumination A and global scattering B + C. Many ray paths can contribute to global light.

direct (D) and global (G) components as

$$D = \frac{L^+ - L^-}{1 - b} \tag{4}$$

$$G = 2\frac{L^- - bL^+}{1 - b^2} \tag{5}$$

Here, b accounts for background illumination. Note that global-direct separation was formulated using ray optics, whereas speckle is a wave phenomenon.

In order to use Eqs. 4 and 5, and avoid including complex diffraction integrals, we apply speckle statistics (derived rigorously from the underlying wave physics [12]). We describe our model in Sec. 3, below.

3. Synthetic Results

3.1. Simulation Methods

We first evaluate the method with synthetic data. Because rendering dynamic volumetric scattering is challenging, we model a two-layer system. The front layer represents the skin, and the rear layer contains all the scattering of the underlying tissue.

To model coherent scattering (speckle), we proceed as follows: first, the front layer is illuminated with a high-frequency speckle pattern, independent of the sample under study. This pattern strikes the first layer, and scattering is modeled by generating a random intensity pattern with negative exponential statistics. The resulting speckle pattern is the direct component. Next, a portion of this pattern is transmitted and scattered towards the rear layer. Propagation is accounted for by blurring each speckle. The rear layer forms a second speckle pattern (global component), which is reflected and added to the direct component.

Dynamic speckle is modeled by averaging S realizations of speckle at a pixel, where S is proportional to the velocity at that pixel [12] and the exposure time: $S = vT \sim T/\tau_c$.

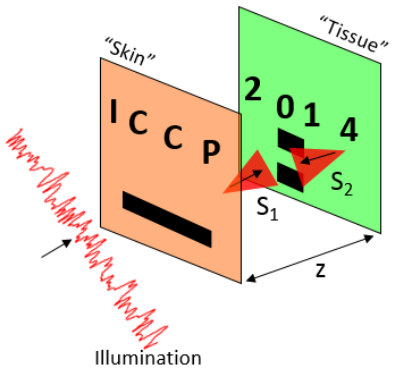

Figure 5. Simulated scene with two scattering layers. The black characters indicate areas of high speed. Incident speckle illumination scatters to the first layer, then to the second. Both are recorded simultaneously for four different incident illumination patterns.

Thus, higher speeds and longer exposure times imply a larger average, which implies a reduced contrast. The simulation is repeated with N independent speckle illumination patterns, and global-direct decomposition is carried out with the N resulting images.

The blur kernel size is chosen to approximate diffraction. In the paraxial approximation, a speckle of size w_0 blurs to $w(z)$ after a distance z according to

$$z = \frac{\pi w_0^2}{\lambda}\sqrt{\left(\frac{w(z)}{w_0}\right)^2 - 1} \tag{6}$$

For example, for an average speckle size of 5 pixels, a blur kernel of 20 pixels, a wavelength of 0.750 μm, and a camera pixel size of 5 μm with unity magnification, Eq. 6 implies that the inter-layer distance is 1 cm, which is a typical quantity in biological imaging.

We note here that the high-frequency illumination pattern is itself a random speckle field. This intuitively "matches" the system dynamics and allows us to ignore diffraction from, e.g., the edges of the more conventional checkerboard pattern. The goal of the method is to calculate a relative speed map of the front layer based on $N = 4$ illumination patterns by removing any corruption from the presence of the rear layer.

3.2. Simulation Results

The synthetic scene is shown schematically in Fig. 5, and results are shown in Fig. 6. Fig. 6a shows the ground truth speed maps of each layer and a synthetic measurement of each layer in the absence of the other. Note the reduced contrast within the characters, where the speed is high. Individual measurements for four illumination patterns are shown in Fig. 6b. Though they appear similar, each one is a result

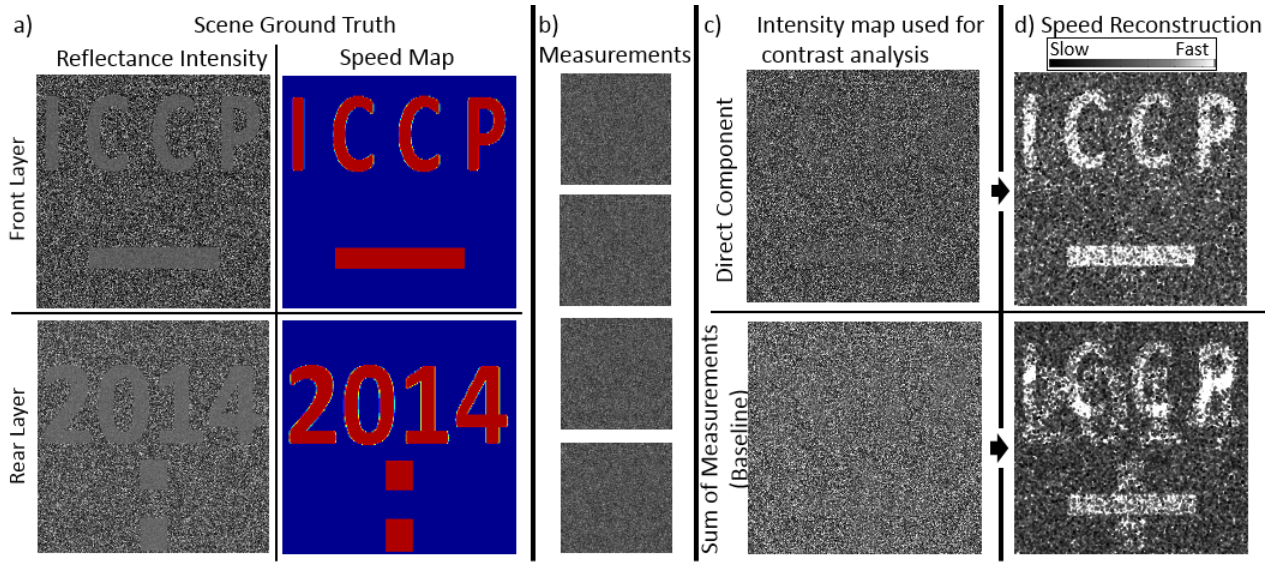

Figure 6. Synthetic results demonstrate benefits of global-direct separation for skin perfusion. (a) Scene ground truth: speed maps indicate areas of relative motion, and reflectance maps indicate the contrast measurement of each layer in the absence of the other. (b) Four measurements, illuminated by different speckle patterns. (c) Decomposition to direct component reflectance (top), the sum of measurements as a baseline (bottom). (d) Speed reconstruction based on the corresponding intensity maps. The reconstruction based on direct component reproduces the speed map of the front layer, whereas the baseline result contains speed contributions from both layers.

of a different speckle illumination pattern. Inputting these measurements into Eqs. 4 and 5, we obtain a direct light image. We reconstruct the speed map based on the contrast of this image (Fig. 6c,d (top)). For comparison (Fig. 6c,d (bottom)), we see that the standard LSCI reconstructs a speed map that contains information from both layers ("ICCP" and "2014"), whereas the global-direct separation successfully decouples them.

To quantify the simulation results, we normalize all speed maps to the total energy of the ground truth speed map. We define total image energy as the total kinetic energy of the individual pixels:

$$E = \sum_{i,j=1}^{n} V_{ij}^2 \tag{7}$$

where V_{ij} is the speed at pixel (i, j), and the image is $n \times n$ pixels. The error metric is

$$e_k = \frac{1}{n^2} \sum_{i,j=1}^{n} \|V_{ij}^{(g)} - V_{ij}^{(k)}\|^2 \tag{8}$$

where $V^{(k)}$ is the reconstructed speed map (direct or baseline), and $V^{(g)}$ is the front layer ground truth speed map.

Fig. 7 (top) shows the reconstruction error as a function of SNR for different numbers of illumination patterns. We see that both the standard LSCI method (red) and our method (blue) improve for increasing N. For $N > 4$, there was no appreciable improvement. With high SNR, our reconstructions produce 50% less error than the baseline LSCI method. Because the direct component is a difference of images (Eq. 4), it is susceptible to noise. Therefore, for low SNR, the two methods are comparable. Interestingly, there is a regime of standard LSCI where increasing SNR increases the reconstruction error. We expect that this is caused by a small amount of noise, which reduces local contrast and changes the effective local speed.

Fig. 7 (bottom) shows analysis of the reconstruction error for varying distance between layers (a larger distance between layers results in more blurring according to Eq. 6). As the distance between the layers increases, the reflected speckle field becomes increasingly blurred, which improves the global-direct separation. On the other hand, the reflections corrupt a wider area of the image and increase the baseline reconstruction error. As N increases, the error is reduced and similarly, above $N > 4$, there is little change.

4. Experimental Validation

4.1. Experimental Prototype

We implement the method in hardware using a Lumenera monochrome camera without an IR filter to image objects approximately 40 cm away with a 50 mm Nikon lens ($f/2.8$). To implement four illumination patterns, we use four light sources: 3 mW lasers of center wavelength 785

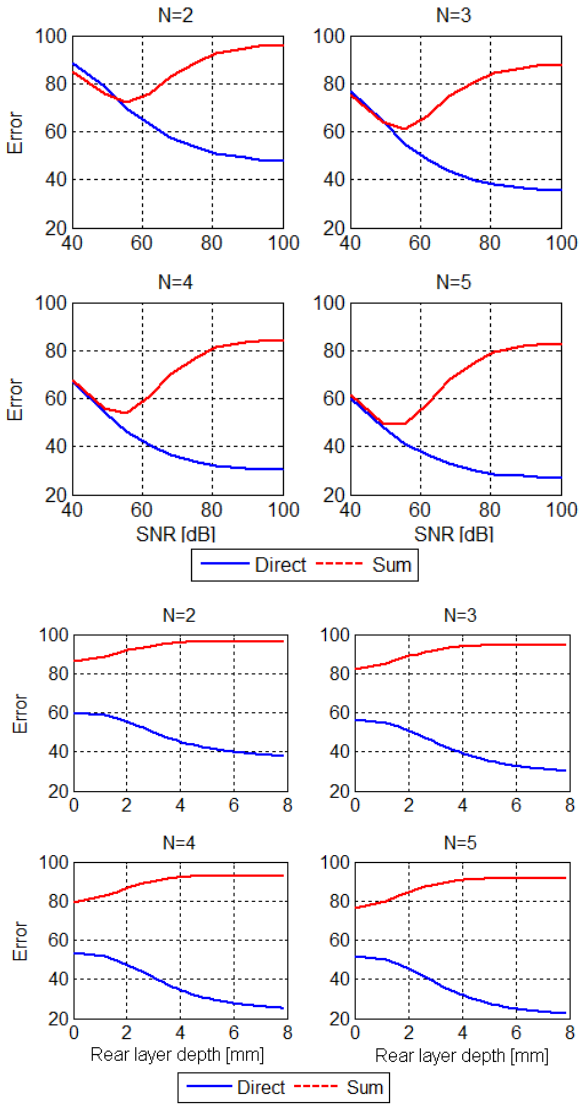

Figure 7. Simulation speed reconstruction error for varying number of illumination sources, measurement noise (top) and internal layer depth (bottom). Each plot shows the reconstruction error using the direct component (solid blue), and using the sum of all measurements (dashed red), for various measurement noise (SNR). N is the number of illumination patterns used.

nm, placed around the camera lens. To create illumination speckle patterns, each laser passes through a diffusive material (duct tape). The lasers are controlled by an Arduino microcontroller, which is synchronized in real time using a Matlab interface (Fig. 8). The lasers illuminate the scene sequentially, and the camera records an image for each one with an exposure time of 50 ms. The total acquisition time is approximately one second. The four recorded images are then used to separate global and direct light. Contrast analysis is performed on the direct light, and the speed map is

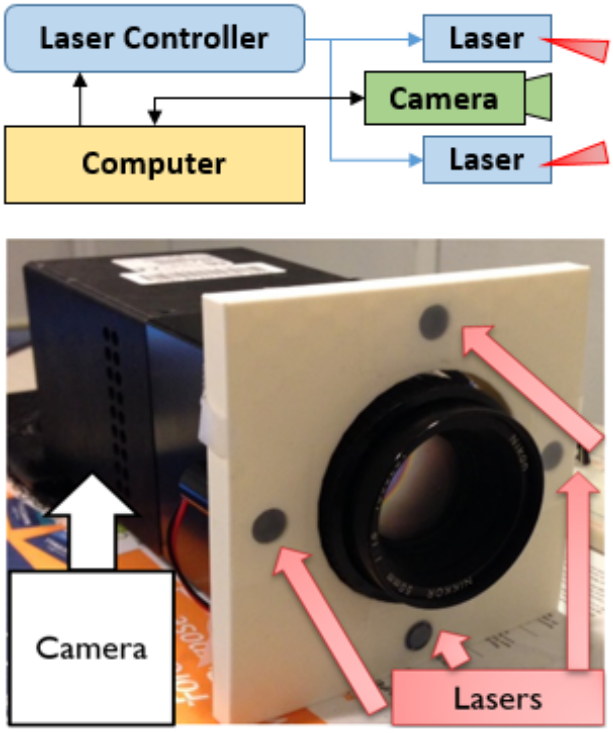

Figure 8. Experimental setup. Top: system block diagram. Bottom: picture of the imaging system used.

reconstructed. To calculate contrast, we use an averaging window of $M = 13$ (c.f., Eq. 1), and the background illumination is $b = 0.01$.

4.2. Experimental Results

The first result is shown in Fig. 1, which shows a healthy human hand. In Fig. 1a, we calculate the speed map using two LSCI methods. The first is a direct contrast calculation from the sum of the four measurements (the sum is used to create a uniform illumination over the full field). The second is normalized by the skin texture. However, both produce similar erroneous results. Skin perfusion in a normal hand should be uniform, whereas the conventional results have a highly uneven distribution. The four illumination measurements and the direct component speed reconstruction are shown in Fig. 1b, where we see a far more uniform speed map.

Our improvement results from the global component (Fig. 1c) being removed and no longer corrupting the skin perfusion measurement. Note that the global component contains no speckle, the direct component does contain speckle, and the conventional measurement contains an intermediate amount. Further inspection of the direct speed map reveals two outliers, the tip of the second finger from the top, and the bottom right part of the palm. These areas

appear to have low speed associated with them. This can be explained by examining the direct intensity map. We notice these areas appear dark, which means they were not directly illuminated during acquisition.

The second result (Fig. 9) shows a finger with a superficial burn on an otherwise healthy finger. Because the burned skin is dead, perfusion there should be low. Indeed, the speed map calculated from the direct component corroborates this. Raw measurements are shown in Fig. 9a, with our reconstruction in Fig. 9b. Here, the burned area is blue (low perfusion), and the rest of the (healthy) finger shows constant perfusion. Interestingly, the burn is almost invisible in the global component (Fig. 9c), and more obvious in the direct component. Baseline conventional methods (non-normalized and normalized) are shown in Figs. 9d,e. The burned area has less contrast, and the healthy finger does not exhibit constant perfusion.

5. Discussion and Future Work

Our results here indicate that global-direct separation methods, derived for ray optics, have potential use for coherent imaging. This can represent a significant advancement for LSCI and can improve reconstructions of blood flow. Here, diffraction is modeled purely as a statistical model, with the resulting high frequency speckle patterns amenable for computational separation, but deterministic scenes (e.g., diffraction from an edge) have not been studied. A first-principles generalization of diffractive global-direct separation, to our knowledge, has yet to be performed. Further, though our qualitative results are similar to those reported in conventional LSCI, we expect that global-direct separation of coherent light can be made quantitative.

The prototype hardware can be improved in several ways. Other optical wavelengths can provide information about, e.g., oxygenated and non-oxygenated red blood cells. Furthermore, a single laser steered by galvanometers would improve stability and repeatability compared to the current multi-laser approach. Replacing the current 50 mm lens with an objective will improve spatial resolution (at the cost of narrowing the field of view). Computationally, different space-time-multiplexing techniques coupled with sparsity-based approaches can be integrated into this approach for more efficient information throughput.

Applying global-direct separation with coherent illumination is not limited to perfusion and can improve other skin-related analyses, such as extracting biological quantities [32] and improving rendering [14]. It can also improve skin lesion analysis and diagnosis [7].

6. Conclusions

We have implemented global-direct illumination separation of coherent speckle patterns for application in skin perfusion analysis. Our interference model is based on speckle intensity statistics and can be used as a starting point for analyzing global-direct separation techniques in the presence of diffraction from rough surfaces. This work serves as an indication that ray-based computational photography techniques have potential for diffraction-based applications. Thus, this contribution offers a bridge between computational photography and biomedical imaging with intuitive modeling of light scattering. Future efforts in computational photography can be applied towards medical imaging of, for example, wound healing, burn recovery, and skin surgeries.

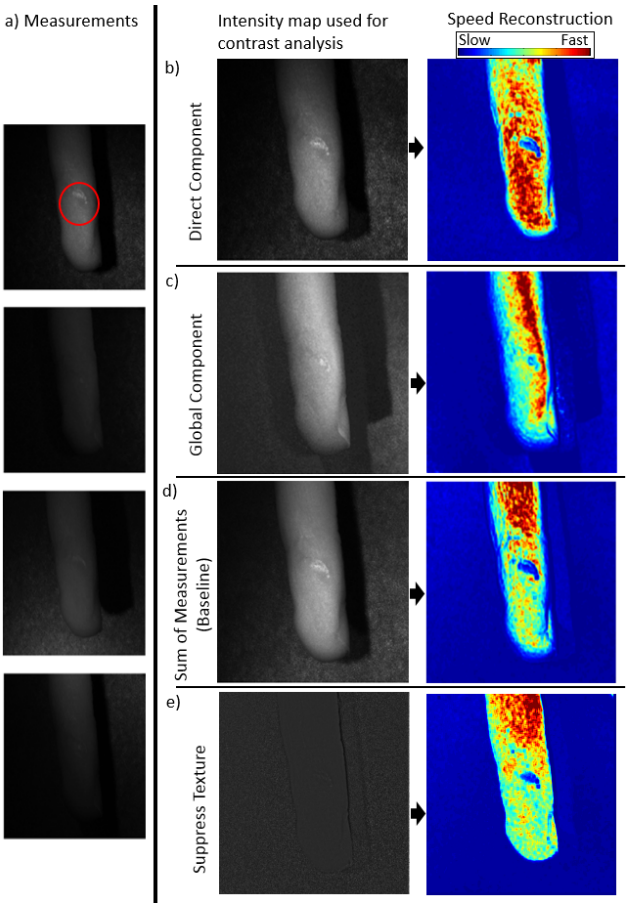

Figure 9. Experimental results demonstrating improvement of skin perfusion measurement of unhealthy skin. a) Four raw measurements of a burned finger (burn is circled in red). The four measurements are decomposed to direct (b) and global (c) components, as well as the sum of measurements for a baseline comparison (d,e). Right column: LSCI analysis results performed on the corresponding intensity maps. The burn is most obvious in the direct component, and is almost invisible in the global component. The direct component also provides more uniform results around the burn.

References

[1] S. Achar, S. T. Nuske, and S. G. Narasimhan. Compensating for Motion During Direct-Global Separation. In *2013 Int. Conf. Comp. Vis.*, 1481–1488, 2013.

[2] D. Briers, D. D. Duncan, E. Hirst, S. J. Kirkpatrick, M. Larsson, W. Steenbergen, T. Stromberg, and O. B. Thompson. Laser speckle contrast imaging: theoretical and practical limitations. *J. Biomed. Opt.*, 18:066018, 2013.

[3] J. D. Briers. Laser Doppler and time-varying speckle: a reconciliation. *J. Opt. Soc. Am. A*, 13:345, 1996.

[4] J. D. Briers and S. Webster. Laser speckle contrast analysis (LASCA): a nonscanning, full-field technique for monitoring capillary blood flow. *J. Biomed. Opt.*, 1:174–9, 1996.

[5] H. Cheng, Q. Luo, Q. Liu, Q. Lu, H. Gong, and S. Zeng. Laser speckle imaging of blood flow in microcirculation. *Phys. Med. Bio.*, 49:1347–1357, 2004.

[6] H. Cheng, Q. Luo, S. Zeng, S. Chen, J. Cen, and H. Gong. Modified laser speckle imaging method with improved spatial resolution. *J. Biomed. Opt.*, 8:559–64, 2003.

[7] S. Cotton, E. Claridge, and P. Hall. A skin imaging method based on a colour formation model and its application to the diagnosis of pigmented skin lesions. In *Proceedings of Medical Image Understanding and Analysis*, 99: 49–52, 1999.

[8] D. D. Duncan and S. J. Kirkpatrick. Can laser speckle flowmetry be made a quantitative tool? *J. Opt. Soc. Am. A*, 25:2088, 2008.

[9] A. Fercher and J. Briers. Flow visualization by means of single-exposure speckle photography. *Opt. Comm.*, 37:326–330, 1981.

[10] I. Fredriksson, M. Larsson, and T. Strömberg. Model-based quantitative laser Doppler flowmetry in skin. *J. Biomed. Opt.*, 15:057002, 2010.

[11] J. W. Goodman. *Laser Speckle and Related Phenomena*. Springer, 1975.

[12] J. W. Goodman. *Speckle Phenomena in Optics: Theory and Applications*. Englewood, CO : Roberts & Co., 2007.

[13] M. Gupta, A. Agrawal, A. Veeraraghavan, and S. G. Narasimhan. Structured light 3D scanning in the presence of global illumination. In *IEEE CVPR*, 713–720, 2011.

[14] J. Jimenez, T. Weyrich, T. Scully, N. Barbosa, C. Donner, X. Alvarez, T. Vieira, P. Matts, V. Orvalho, and D. Gutierrez. A practical appearance model for dynamic facial color. *ACM Trans. Graph.*, 29:1, 2010.

[15] A. Kadambi, H. Ikoma, X. Lin, G. Wetzstein, and R. Raskar. Subsurface Enhancement through Sparse Representations of Multispectral Direct/Global Decomposition. In *OSA: Imaging and Applied Optics*, CTh1B.4, 2013.

[16] T. Kobayashi, M. Gupta, and S. K. Nayar. Multiplexed illumination for scene recovery in the presence of global illumination. In *IEEE Int. Conf. Comp. Vis.*, 691–698, 2011.

[17] M. Le Thinh, J. S. Paul, H. Al-Nashash, A. Tan, A. R. Luft, F. S. Sheu, and S. H. Ong. New insights into image processing of cortical blood flow monitors using laser speckle imaging. *IEEE Trans. Med. Imag.*, 26:833–42, 2007.

[18] P. Li, S. Ni, L. Zhang, S. Zeng, and Q. Luo. Imaging cerebral blood flow through the intact rat skull with temporal laser speckle imaging. *Opt. Lett.*, 31:1824, 2006.

[19] T. Loupas, W. McDicken, and P. Allan. An adaptive weighted median filter for speckle suppression in medical ultrasonic images. *IEEE Trans. Circ. Sys.*, 36:129–135, 1989.

[20] J. K. Meisner, S. Sumer, K. P. Murrell, T. J. Higgins, and R. J. Price. Laser speckle flowmetry method for measuring spatial and temporal hemodynamic alterations throughout large microvascular networks. *Microcirculation*, 19:619–31, 2012.

[21] S. K. Nayar, G. Krishnan, M. D. Grossberg, and R. Raskar. Fast separation of direct and global components of a scene using high frequency illumination. *ACM Trans. Graph.*, 25:935, 2006.

[22] M. O'Toole, R. Raskar, and K. N. Kutulakos. Primal-dual coding to probe light transport. *ACM Trans. Graph.*, 31:1–11, 2012.

[23] A. B. Parthasarathy, W. J. Tom, A. Gopal, X. Zhang, and A. K. Dunn. Robust flow measurement with multi-exposure imaging. *Opt. Expr.*, 16:1975–1989, 2008.

[24] Perimed (R). PeriCam PSI System http://www.perimed-instruments.com/.

[25] J. Qin, R. Reif, Z. Zhi, S. Dziennis, and R. Wang. Hemodynamic and morphological vasculature response to a burn monitored using a combined dual-wavelength laser speckle and optical microangiography imaging system. *Biomed. Opt. Expr.*, 3:455–66, 2012.

[26] A. Rege, J. Senarathna, N. Li, and N. V. Thakor. Anisotropic processing of laser speckle images improves spatiotemporal resolution. *IEEE Trans. Biomed. Eng.*, 59:1272–80, 2012.

[27] J. M. Schmitt, S. H. Xiang, and K. M. Yung. Speckle in optical coherence tomography. *J. Biomed. Opt*, 4:95–101, 1999.

[28] J. Senarathna, A. Rege, N. Li, and N. V. Thakor. Laser Speckle Contrast Imaging: theory, instrumentation and applications. *IEEE Rev. Biomed Eng.*, 6:99–110, 2013.

[29] M. S. D. Smith, E. F. Packulak, and M. G. Sowa. Development of a laser speckle imaging system for measuring relative blood flow velocity. 6343: 634304, 2006.

[30] C. J. Stewart, C. L. Gallant-Behm, K. Forrester, J. Tulip, D. A. Hart, and R. C. Bray. Kinetics of blood flow during healing of excisional full-thickness skin wounds in pigs as monitored by laser speckle perfusion imaging. *Skin Res. Technol.*, 12:247–53, 2006.

[31] O. Thompson, J. Bakker, C. Kloeze, E. Hondebrink, and W. Steenbergen. Experimental comparison of perfusion imaging systems using multi-exposure laser speckle, single-exposure laser speckle, and full-field laser Doppler. In *Dyn. Fluctuations Biomed. Photonics IX*, 822204, 2012.

[32] N. Tsumura, N. Ojima, K. Sato, M. Shiraishi, H. Shimizu, H. Nabeshima, S. Akazaki, K. Hori, and Y. Miyake. Image-based skin color and texture analysis/synthesis by extracting hemoglobin and melanin information in the skin. In *ACM Trans. Graph. (SIGGRAPH 2003)*, 770, 2003.

[33] L. Wang, J. Xia, J. Yao, K. I. Maslov, and L. V. Wang. Ultrasonically encoded photoacoustic flowgraphy in biological tissue. *Phys. Rev. Lett.*, 111:204301, 2013.

[34] P. Zakharov, A. Völker, A. Buck, B. Weber, and F. Scheffold. Quantitative modeling of laser speckle imaging. *Opt. Lett*, 31:3465, 2006.